Front. Phys. 13(1), 130302 (2018)
DOI 10.1007/s11467-017-0706-6

RESEARCH ARTICLE

Clock frequency estimation under spontaneous emission

Xi-Zhou Qin (秦锡洲)[1], **Jia-Hao Huang** (黄嘉豪)[1], **Hong-Hua Zhong** (钟宏华)[1], **Chaohong Lee** (李朝红)[1,2,†]

[1] *TianQin Research Center & School of Physics and Astronomy, Sun Yat-Sen University (Zhuhai Campus), Zhuhai 519082, China*
[2] *Key Laboratory of Optoelectronic Materials and Technologies, Sun Yat-Sen University (Guangzhou Campus), Guangzhou 510275, China*
Corresponding author. E-mail: [†]*lichaoh2@mail.sysu.edu.cn*
Received March 20, 2017; accepted June 26, 2017

We investigate the quantum dynamics of a driven two-level system under spontaneous emission and its application in clock frequency estimation. By using the Lindblad equation to describe the system, we analytically obtain its exact solutions, which show three different regimes: Rabi oscillation, damped oscillation, and overdamped decay. From the analytical solutions, we explore how the spontaneous emission affects the clock frequency estimation. We find that under a moderate spontaneous emission rate, the transition frequency can still be inferred from the Rabi oscillation. Our results enable potential practical applications in frequency measurement and quantum control under decoherence.

Keywords clock frequency estimation, two-level system, spontaneous emission

PACS numbers 03.65.Yz, 42.50.Ct, 06.20.-f

1 Introduction

Clock frequency estimation forms the basis of the physics for precision measurements [1–3], spectroscopy [4], and astronomy [5]. It is also at the heart of modern technologies, from the global positioning system (GPS) [6] and magnetometers [7, 8] to inertial sensors [7] (e.g., gyroscopes and gravimeters). A two-level system (TLS) coupled with an oscillating field is the prototype of a clock. This may correspond to an ensemble of atoms or ions driven by an electromagnetic field in the microwave, optical, or ultraviolet regions. The TLS ticks with the oscillations of the electromagnetic waves whose frequency is locked to that of the energy difference between two discrete levels. The closer the external field frequency is to the transition frequency of the TLS, the larger the contrast of the Rabi oscillation. Hence, the clock frequency can be estimated according to the population dynamics of the TLS. This model was first proposed by Rabi [9] and widely used in atomic clocks [10–12].

The performances of an atomic clock are affected by many factors [13–15]. In realistic experiments, decoherence is unavoidable and plays an important role, especially when the uncertainty is at the level of 10^{-17} [16, 17] or even smaller [18]. For an atomic clock, one of the essential mechanisms of decoherence is spontaneous emission. The effects of spontaneous emission may have great influence on the population dynamics of the TLS and eventually degrade the performance of the clock. Therefore, it is of great interest to investigate how the spontaneous emission affects the population dynamics and clock frequency estimation.

Theoretically, a TLS driven by an oscillating field under spontaneous emission is described well by the Lindblad equation [19]. Although the driven TLSs have been extensively investigated, the search for exactly solvable, driven TLSs is still an active field [20]. Two famous examples of solvable driven TLSs are the Landau–Zener [21, 22] and Rabi [9] problems. Solvable models of driven TLSs provide the most reliable explanations for experimental observations as well as numerical calculations in quantum optics [23–26], quantum metrology [27–30], and quantum control [31–35]. Among the existing analytical methods for solving TLSs [20, 36–41], much attention has been given to the driven TLS described by the Schrödinger equations, which fail to include the spontaneous emission. Solvable driven TLSs obeying the Lindblad equation [42, 43] are still rare (see Ref. [44] for a review on dissipative driven TLSs). Furthermore, the

*arXiv: 1707.03958.

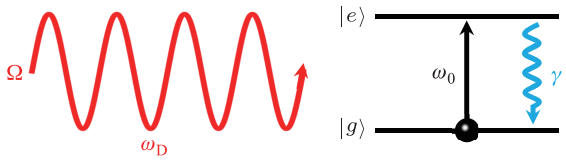

Fig. 1 Schematic of a TLS coupled with an oscillating electromagnetic field under spontaneous emission. Here, Ω and ω_D are the Rabi and oscillation frequencies of the driving field, respectively, ω_0 is the transition frequency of the TLS, and γ represents the spontaneous emission rate.

analytical study of decoherence is always difficult and nontrivial for practical applications [34, 45–48].

Here, we study a TLS driven by an oscillating field under spontaneous emission. Within the Markovian approximation, the system can be described by the Lindblad master equation. Then, we solve the Lindblad equation analytically and obtain its exact solutions. We analyze different regimes for the population dynamics and investigate the clock frequency estimation in the presence of spontaneous emission. Our analytical results illustrate that the spontaneous emission does not induce any frequency shift but the estimated precision of the transition frequency would be reduced.

This article is organized as follows. In Section 2, we derive the Bloch equations for our system. In Section 2.1, by implementing a linear transformation, we obtain ordinary differential equations with constant coefficients for the system. In Sections 2.2 and 2.3, we determine the analytical solutions for the Lindblad equation. In Section 3, we discuss the population dynamics and clock frequency estimation in the presence of spontaneous emission. Finally, a brief summary of our results is presented in Section 4.

2 Lindblad equation and its analytical solutions

We consider two stable states $|g\rangle$ and $|e\rangle$ in an atomic clock. By introducing the pseudospin-1/2 operators $\hat{S}^+ = |e\rangle\langle g|$, $\hat{S}^- = |g\rangle\langle e|$, $\hat{S}^x = \frac{1}{2}(\hat{S}^+ + \hat{S}^-)$, $\hat{S}^y = \frac{1}{2\mathrm{i}}(\hat{S}^+ - \hat{S}^-)$, and $\hat{S}^z = \frac{1}{2}(|e\rangle\langle e| - |g\rangle\langle g|)$, within the Markovian approximations, the density matrix operator of the system, $\hat{\rho}(t)$, is governed by the Lindblad equation (throughout this article, we set $\hbar = 1$):

$$\frac{\mathrm{d}}{\mathrm{d}t}\hat{\rho}(t) = -\mathrm{i}[\hat{H}(t), \hat{\rho}(t)] + \mathcal{L}[\hat{\rho}(t)]. \tag{1}$$

The time-dependent Hamiltonian can be expressed as

$$\hat{H}(t) = \hat{H}_0 + \hat{H}_1(t), \tag{2}$$

$$\hat{H}_0 = \omega_0 \hat{S}^z, \tag{3}$$

$$\hat{H}_1(t) = \Omega[\hat{S}^x \cos(\omega_D t) + \hat{S}^y \sin(\omega_D t)], \tag{4}$$

where $\hat{H}_0$ is the Hamiltonian of the TLS with transition frequency ω_0 and $\hat{H}_1(t)$ corresponds to the coupling between the TLS and the external electromagnetic field with Rabi frequency Ω and driving frequency ω_D. The schematic is shown in Fig. 1. Here, $\mathcal{L}$ is a superoperator that describes the spontaneous emission [42, 43]:

$$\mathcal{L}[\hat{\rho}] = \gamma(\hat{S}^-\hat{\rho}\hat{S}^+ - \frac{1}{2}\hat{S}^+\hat{S}^-\hat{\rho} - \frac{1}{2}\hat{\rho}\hat{S}^+\hat{S}^-), \tag{5}$$

with γ being the spontaneous emission rate.

In this article, we derive the equations in the Dirac picture. By applying the transformation $\hat{\rho}^D(t) = \mathrm{e}^{\mathrm{i}\hat{H}_0 t}\hat{\rho}(t)\mathrm{e}^{-\mathrm{i}\hat{H}_0 t}$, the Lindblad equation (1) becomes

$$\frac{\mathrm{d}}{\mathrm{d}t}\hat{\rho}^D(t) = -\mathrm{i}[\hat{H}_1^D(t), \hat{\rho}^D(t)] + \mathcal{L}^D[\hat{\rho}^D(t)]. \tag{6}$$

Here, by using the identity $\mathrm{e}^{\mathrm{i}\hat{H}_0 t}\hat{S}^\pm\mathrm{e}^{-\mathrm{i}\hat{H}_0 t} = \mathrm{e}^{\pm\mathrm{i}\omega_0 t}\hat{S}^\pm$,

$$\hat{H}_1^D(t) = \frac{1}{2}\Omega(\hat{S}^+\mathrm{e}^{-\mathrm{i}\Delta t} + \hat{S}^-\mathrm{e}^{\mathrm{i}\Delta t}) \tag{7}$$

and

$$\mathcal{L}^D[\hat{\rho}^D] = \gamma\left(\hat{S}^-\hat{\rho}^D\hat{S}^+ - \frac{1}{2}\hat{S}^+\hat{S}^-\hat{\rho}^D - \frac{1}{2}\hat{\rho}^D\hat{S}^+\hat{S}^-\right), \tag{8}$$

where the detuning is defined as $\Delta = \omega_D - \omega_0$. Equation (6), based on the eigenstates of $\hat{S}^z$, becomes

$$\begin{cases} \frac{\mathrm{d}}{\mathrm{d}t}\rho^{D00} = \frac{1}{2\mathrm{i}}\Omega(\mathrm{e}^{-\mathrm{i}\Delta t}\rho^{D10} - \mathrm{e}^{\mathrm{i}\Delta t}\rho^{D01}) - \gamma\rho^{D00}, \\ \frac{\mathrm{d}}{\mathrm{d}t}\rho^{D01} = \frac{1}{2\mathrm{i}}\Omega\mathrm{e}^{-\mathrm{i}\Delta t}(\rho^{D11} - \rho^{D00}) - \frac{1}{2}\gamma\rho^{D01}, \\ \frac{\mathrm{d}}{\mathrm{d}t}\rho^{D10} = -\frac{1}{2\mathrm{i}}\Omega\mathrm{e}^{\mathrm{i}\Delta t}(\rho^{D11} - \rho^{D00}) - \frac{1}{2}\gamma\rho^{D10}, \\ \frac{\mathrm{d}}{\mathrm{d}t}\rho^{D11} = -\frac{1}{2\mathrm{i}}\Omega(\mathrm{e}^{-\mathrm{i}\Delta t}\rho^{D10} - \mathrm{e}^{\mathrm{i}\Delta t}\rho^{D01}) + \gamma\rho^{D00}, \end{cases} \tag{9}$$

with

$$\rho^D(t) = \begin{pmatrix} \rho^{D00}(t) & \rho^{D01}(t) \\ \rho^{D10}(t) & \rho^{D11}(t) \end{pmatrix}. \tag{10}$$

Next, introducing the Bloch vector, $\boldsymbol{R} = (u, v, w)^{\mathrm{T}}$ (where the superscript "T" denotes the matrix transpose operation), the density matrix can be written as

$$\hat{\rho}^D = \frac{1}{2}(\hat{1} + u\hat{\sigma}^x + v\hat{\sigma}^y + w\hat{\sigma}^z), \tag{11}$$

where $\hat{\sigma}^x$, $\hat{\sigma}^y$, and $\hat{\sigma}^z$ are the Pauli matrices. The three coefficients can be expressed in the form of

$$\begin{cases} u = \mathrm{tr}[\hat{\rho}^D\hat{\sigma}^x] = \cos(\omega_0 t)\langle\hat{\sigma}^x\rangle + \sin(\omega_0 t)\langle\hat{\sigma}^y\rangle, \\ v = \mathrm{tr}[\hat{\rho}^D\hat{\sigma}^y] = -\sin(\omega_0 t)\langle\hat{\sigma}^x\rangle + \cos(\omega_0 t)\langle\hat{\sigma}^y\rangle, \\ w = \mathrm{tr}[\hat{\rho}^D\hat{\sigma}^z] = \langle\hat{\sigma}^z\rangle. \end{cases} \tag{12}$$

Here, $\langle\hat{\sigma}^{\alpha}\rangle = \mathrm{tr}[\hat{\rho}(t)\hat{\sigma}^{\alpha}]$ is the expectation value of $\hat{\sigma}^{\alpha}$ for the evolved state $\hat{\rho}(t)$ ($\alpha = x, y, z$). Then, we obtain the Bloch equations:

$$\begin{cases} \frac{\mathrm{d}}{\mathrm{d}t}u = -\frac{1}{2}\gamma u + \Omega\sin(\Delta t)w, \\ \frac{\mathrm{d}}{\mathrm{d}t}v = -\frac{1}{2}\gamma v - \Omega\cos(\Delta t)w, \\ \frac{\mathrm{d}}{\mathrm{d}t}w = -\Omega\sin(\Delta t)u + \Omega\cos(\Delta t)v - \gamma w - \gamma. \end{cases} \tag{13}$$

The Bloch equations (13) can be written in a more compact form:

$$\frac{\mathrm{d}}{\mathrm{d}t}\boldsymbol{R} = \boldsymbol{M}\boldsymbol{R} + \boldsymbol{R}_0, \tag{14}$$

where $\boldsymbol{R}_0 = -\gamma(0,0,1)^{\mathrm{T}}$ and the coefficient matrix is defined as

$$\boldsymbol{M} = \begin{pmatrix} -\frac{1}{2}\gamma & 0 & \Omega\sin(\Delta t) \\ 0 & -\frac{1}{2}\gamma & -\Omega\cos(\Delta t) \\ -\Omega\sin(\Delta t) & \Omega\cos(\Delta t) & -\gamma \end{pmatrix}. \tag{15}$$

2.1 Linear transformation

In general, when the coefficient matrix $\boldsymbol{M}$ is time-dependent, it is not easy to solve the Bloch equation (14) directly. Such differential equations with periodically oscillating coefficients can be treated with Floquet theory [49]. However, the obtained solutions are usually given in the form of a series, which may be sometimes inconvenient. Here, we present another simpler approach, which enables us to obtain the complete and analytical solutions in closed-form expressions.

First, we take a general reversible linear transformation of the Bloch vectors:

$$\boldsymbol{R} = \boldsymbol{P}\boldsymbol{R}^{Q}, \tag{16}$$

where $\boldsymbol{R}^{Q} = (u^{Q}, v^{Q}, w^{Q})^{\mathrm{T}}$ is a new set of variables and $\boldsymbol{P}$ is an undetermined 3×3 matrix with time-dependent matrix elements. Meanwhile, Eq. (14) becomes

$$\frac{\mathrm{d}}{\mathrm{d}t}\boldsymbol{R}^{Q} = \boldsymbol{F}\boldsymbol{R}^{Q} + \boldsymbol{G}, \tag{17}$$

with

$$\boldsymbol{F} = \boldsymbol{P}^{-1}\boldsymbol{M}\boldsymbol{P} - \boldsymbol{P}^{-1}\frac{\mathrm{d}}{\mathrm{d}t}\boldsymbol{P}, \tag{18}$$

$$\boldsymbol{G} = \boldsymbol{P}^{-1}\boldsymbol{R}_0. \tag{19}$$

The differential equation (17) can be simplified into a linear one with constant coefficients if $\boldsymbol{F}$ is time-independent, or equivalently $\frac{\mathrm{d}}{\mathrm{d}t}\boldsymbol{F} = 0$. To let $\frac{\mathrm{d}}{\mathrm{d}t}\boldsymbol{F} = 0$, it is not unique to choose the transformation matrix $\boldsymbol{P}$. Here, as an example, we set $\boldsymbol{P}$ to the form of

$$\boldsymbol{P} = \mathrm{e}^{-\gamma t}\begin{pmatrix} \cos(\Delta t) & -\sin(\Delta t) & 0 \\ \sin(\Delta t) & \cos(\Delta t) & 0 \\ 0 & 0 & 1 \end{pmatrix}, \tag{20}$$

according to $\boldsymbol{M}$ (15). Substituting $\boldsymbol{P}$ (20) into Eq. (18), one can easily obtain

$$\boldsymbol{F} = \begin{pmatrix} \frac{1}{2}\gamma & \Delta & 0 \\ -\Delta & \frac{1}{2}\gamma & -\Omega \\ 0 & \Omega & 0 \end{pmatrix} \tag{21}$$

and $\boldsymbol{G} = -\gamma\mathrm{e}^{\gamma t}(0,0,1)^{\mathrm{T}}$, respectively. Here, $\boldsymbol{F}$ satisfies the desired condition $\frac{\mathrm{d}}{\mathrm{d}t}\boldsymbol{F} = 0$. Thus far, we have simplified the Bloch equation (14) by a straight linear transformation and the new differential equation can be solved much more easily.

2.2 Solutions with zero detuning

At resonance $\omega_D = \omega_0$ (i.e., zero detuning $\Delta = 0$), Eq. (17) can be reduced to

$$\begin{cases} \frac{\mathrm{d}}{\mathrm{d}t}u^{Q} = \frac{1}{2}\gamma u^{Q}, \\ \frac{\mathrm{d}}{\mathrm{d}t}v^{Q} = \frac{1}{2}\gamma v^{Q} - \Omega w^{Q}, \\ \frac{\mathrm{d}}{\mathrm{d}t}w^{Q} = \Omega v^{Q} - \gamma\mathrm{e}^{\gamma t}. \end{cases} \tag{22}$$

In this case, it is easy to find that $u^{Q}(t) = u_0\mathrm{e}^{\frac{1}{2}\gamma t}$, $v^{Q}(t) = \frac{1}{\Omega}[\frac{\mathrm{d}}{\mathrm{d}t}w^{Q}(t) + \gamma\mathrm{e}^{\gamma t}]$, and

$$\frac{\mathrm{d}^2}{\mathrm{d}t^2}w^{Q}(t) - \frac{1}{2}\gamma\frac{\mathrm{d}}{\mathrm{d}t}w^{Q}(t) + \Omega^2 w^{Q}(t) + \frac{1}{2}\gamma^2\mathrm{e}^{\gamma t} = 0. \tag{23}$$

A special solution to Eq. (23) is $w_s^{Q}(t) = -\frac{\gamma^2}{\gamma^2+2\Omega^2}\mathrm{e}^{\gamma t}$. The characteristic equation of Eq. (23) is

$$\lambda^2 - \frac{1}{2}\gamma\lambda + \Omega^2 = 0. \tag{24}$$

We denote the discriminant of (24) as $D_0 = \frac{1}{4}\gamma^2 - 4\Omega^2$, then, the general solution of Eq. (23) is as follows:
(i) for $D_0 > 0$ ($\gamma > 4\Omega$),

$$w^{Q}(t) = C_1\mathrm{e}^{\lambda_1 t} + C_2\mathrm{e}^{\lambda_2 t} + w_s^{Q}(t); \tag{25}$$

(ii) for $D_0 = 0$ ($\gamma = 4\Omega$),

$$w^{Q}(t) = \mathrm{e}^{\eta t}(C_1 + C_2 t) + w_s^{Q}(t); \tag{26}$$

(iii) for $D_0 < 0$ ($0 \le \gamma < 4\Omega$),

$$w^{Q}(t) = e^{\eta t}[C_1\cos(\omega t) + C_2\sin(\omega t)] + w_s^{Q}(t). \tag{27}$$

Here, in Eq. (25), $\lambda_{1,2}=\frac{1}{4}\gamma\pm\frac{1}{2}\sqrt{D_0}$ ($\lambda_1>\lambda_2$) are two distinct roots of Eq. (24); in Eq. (26), $\eta=\frac{1}{4}\gamma$ is the double root; and in Eq. (27), $\eta\pm\mathrm{i}\omega=\frac{1}{4}\gamma\pm\mathrm{i}\frac{1}{2}\sqrt{-D_0}$ are two conjugate complex roots ($\eta=\frac{1}{4}\gamma$ and $\omega=\frac{1}{2}\sqrt{-D_0}$). The coefficients ($C_1$, C_2) appearing in Eqs. (25)–(27) are determined via the initial conditions (see Appendix A). Thus far, we have completely solved the Bloch equation (14) in the zero-detuning case ($\Delta=0$).

2.3 Solutions with nonzero detuning

For the case of nonzero detuning ($\Delta\neq0$), Eq. (17) becomes

$$\begin{cases}\dfrac{\mathrm{d}}{\mathrm{d}t}u^Q=\dfrac{1}{2}\gamma u^Q+\Delta v^Q,\\ \dfrac{\mathrm{d}}{\mathrm{d}t}v^Q=-\Delta u^Q+\dfrac{1}{2}\gamma v^Q-\Omega w^Q,\\ \dfrac{\mathrm{d}}{\mathrm{d}t}w^Q=\Omega v^Q-\gamma\mathrm{e}^{\gamma t}.\end{cases}\tag{28}$$

Here, we have $v^Q(t)=\frac{1}{\Omega}[\frac{\mathrm{d}}{\mathrm{d}t}w^Q(t)+\gamma\mathrm{e}^{\gamma t}]$, $u^Q(t)=\frac{1}{\Delta\Omega}[-\frac{\mathrm{d}^2}{\mathrm{d}t^2}w^Q(t)+\frac{1}{2}\gamma\frac{\mathrm{d}}{\mathrm{d}t}w^Q(t)-\Omega^2w^Q(t)-\frac{1}{2}\gamma^2\mathrm{e}^{\gamma t}]$, and

$$\frac{\mathrm{d}^3}{\mathrm{d}t^3}w^Q(t)-\gamma\frac{\mathrm{d}^2}{\mathrm{d}t^2}w^Q(t)+(\Delta^2+\Omega^2+\frac{1}{4}\gamma^2)\frac{\mathrm{d}}{\mathrm{d}t}w^Q(t)-\frac{1}{2}\Omega^2\gamma w^Q(t)+\gamma\left(\Delta^2+\frac{1}{4}\gamma^2\right)\mathrm{e}^{\gamma t}=0.\tag{29}$$

A special solution to Eq. (29) is $w_s^Q(t)=-\frac{4\Delta^2+\gamma^2}{4\Delta^2+\gamma^2+2\Omega^2}\mathrm{e}^{\gamma t}$. The characteristic equation of Eq. (29) is

$$\lambda^3-\gamma\lambda^2+\left(\Delta^2+\Omega^2+\frac{1}{4}\gamma^2\right)\lambda-\frac{1}{2}\Omega^2\gamma=0.\tag{30}$$

If we let $\lambda=\lambda'+\frac{1}{3}\gamma$, the characteristic equation (30) becomes

$$\lambda'^3+p\lambda'+q=0,\tag{31}$$

with $p=\Delta^2+\Omega^2-\frac{1}{12}\gamma^2$ and $q=\frac{1}{108}\gamma(36\Delta^2-18\Omega^2+\gamma^2)$. We denote the discriminant of (31) as $D=\frac{1}{4}q^2+\frac{1}{27}p^3=\frac{1}{432}[\Delta^2\gamma^4+(8\Delta^4-20\Delta^2\Omega^2-\Omega^4)\gamma^2+16(\Delta^2+\Omega^2)^3]$; then, the general solution of Eq. (29) is as follows:
(i) for $D=0$ and $p=0$,

$$w^Q(t)=e^{\lambda_1 t}(C_1+C_2t+C_3t^2)+w_s^Q(t);\tag{32}$$

(ii) for $D=0$ and $p\neq0$,

$$w^Q(t)=C_1\mathrm{e}^{\lambda_1 t}+\mathrm{e}^{\lambda_2 t}(C_2+C_3t)+w_s^Q(t);\tag{33}$$

(iii) for $D<0$,

$$w^Q(t)=C_1\mathrm{e}^{\lambda_1 t}+C_2\mathrm{e}^{\lambda_2 t}+C_3\mathrm{e}^{\lambda_3 t}+w_s^Q(t);\tag{34}$$

(iv) for $D>0$,

$$w^Q(t)=C_1\mathrm{e}^{\lambda_1 t}+\mathrm{e}^{\eta t}[C_2\cos(\omega t)+C_3\sin(\omega t)]+w_s^Q(t).\tag{35}$$

Here, in Eq. (32), $\lambda_1=\frac{1}{3}\gamma$ is the triple root of Eq. (30); in Eq. (33), $\lambda_1=\frac{1}{3}\gamma-(4q)^{1/3}$ is the single root and $\lambda_2=\frac{1}{3}\gamma+(\frac{1}{2}q)^{1/3}$ is the double root; in Eq. (34), $\lambda_1=\frac{1}{3}\gamma+r\cos(\frac{1}{3}\phi)$, $\lambda_2=\frac{1}{3}\gamma+r\cos[\frac{1}{3}(\phi+2\pi)]$, and $\lambda_3=\frac{1}{3}\gamma+r\cos[\frac{1}{3}(\phi-2\pi)]$ are the three distinct real roots [where $r=2(-\frac{1}{3}p)^{1/2}$ and $\phi=\arccos(-4qr^{-3})$]; in Eq. (35), $\lambda_1=\frac{1}{3}\gamma+R_1+R_2$ is the real root while $\eta\pm i\omega$ are the two conjugate complex roots with $\eta=\frac{1}{3}\gamma-\frac{1}{2}(R_1+R_2)$ and $\omega=\frac{\sqrt{3}}{2}(R_1-R_2)$ [where $R_1=(-\frac{1}{2}q+\sqrt{D})^{1/3}$ and $R_2=(-\frac{1}{2}q-\sqrt{D})^{1/3}$]. The coefficients ($C_1$, C_2, C_3) appearing in Eqs. (32)–(35) are determined via the initial conditions (see Appendix B). Thus far, we have completely solved the Bloch equation (14) in the nonzero-detuning case ($\Delta\neq0$).

3 Clock frequency estimation

In the previous section, we mathematically solved the Bloch equation (14) for both zero ($\Delta=0$) and nonzero ($\Delta\neq0$) detuning cases and determined their exact analytical solutions. In this section, we mainly discuss the physics behind the analytical solutions and show how the spontaneous emission affects the clock frequency estimation within our model.

3.1 Rabi oscillating, damped oscillating, and overdamping regimes

In the absence of spontaneous emission ($\gamma=0$), the TLS performs the Rabi oscillation. The population difference $w(t)$ evolves as

$$w(t)=\frac{1}{\omega_{\mathrm{R}}^2}\Big[\Delta(-\Omega u_0+\Delta w_0)+\omega_{\mathrm{R}}\Omega v_0\sin(\omega_{\mathrm{R}}t)+\Omega(\Delta u_0+\Omega w_0)\cos(\omega_{\mathrm{R}}t)\Big],\tag{36}$$

with the total Rabi frequency $\omega_{\mathrm{R}}=\sqrt{\Delta^2+\Omega^2}$. For the initial state $\rho(0)=|g\rangle\langle g|$, one has $\rho^{\mathrm{D}}(0)=\rho(0)$ and $(u_0,v_0,w_0)^{\mathrm{T}}=(0,0,-1)^{\mathrm{T}}$. The solution for $w(t)$ (36) is reduced to

$$w(t)=-\frac{\Delta^2}{\omega_{\mathrm{R}}^2}-\frac{\Omega^2}{\omega_{\mathrm{R}}^2}\cos(\omega_{\mathrm{R}}t).\tag{37}$$

The excited population in $|e\rangle$ is given as

$$P_e(t)=\frac{1+w(t)}{2}=\frac{\Omega^2}{\omega_{\mathrm{R}}^2}\sin^2\left(\frac{\omega_{\mathrm{R}}t}{2}\right),\tag{38}$$

which is consistent with the well-known Rabi oscillation.

In the presence of spontaneous emission ($\gamma \neq 0$), there are two types of solutions corresponding to the damped oscillating and overdamping regimes. In the damped oscillating regime, the excited population oscillates with damped amplitude, while in the overdamping regime, the excited population decays exponentially. These two regimes can be distinguished by the discriminant of the characteristic equation.

For $D_0 < 0$ with $\Delta = 0$ or $D > 0$ with $\Delta \neq 0$, the system is in the damped oscillating regime. On the contrary, for $D_0 \geq 0$ with $\Delta = 0$ or $D \leq 0$ with $\Delta \neq 0$, the system is in the overdamping regime. After some algebra, the criteria for determining the damped oscillating regime can be summarized as

$$\Delta^2\gamma^4+(8\Delta^4-20\Delta^2\Omega^2-\Omega^4)\gamma^2+16(\Delta^2+\Omega^2)^3>0. \quad (39)$$

Otherwise, when Eq. (39) is violated, the system is in the overdamping regime. In Fig. 2, we present the phase diagram of the Rabi oscillating, damped oscillating, and overdamping regimes. The damped oscillating regime is colored in blue and bounded by four curves:
(i) the black line,

$$\gamma = 0; \quad (40)$$

(ii) the yellow curve b_2 ($0 \leq |\Delta/\Omega| \leq \frac{1}{2\sqrt{2}}$),

$$\gamma = \sqrt{14\Omega^2 - 4\Delta^2 + 4\Omega\frac{\Omega^2-8\Delta^2}{\Omega+\sqrt{\Omega^2-8\Delta^2}}}; \quad (41)$$

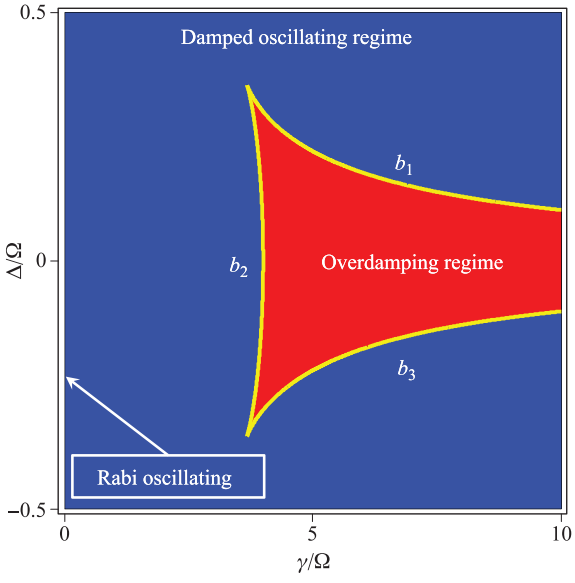

Fig. 2 Phase diagram of three different types of solutions. The black line lying at $\gamma/\Omega = 0$ represents the Rabi oscillating solutions. The blue area is the damped oscillating regime. The red area, as well as the yellow curves b_1, b_2, and b_3, denote the overdamping regime.

(iii), (iv) the yellow curves b_1 ($\Delta > 0$) and b_3 ($\Delta < 0$) (both with $0 < |\Delta/\Omega| \leq \frac{1}{2\sqrt{2}}$), respectively,

$$\gamma = \sqrt{14\Omega^2 - 4\Delta^2 + 4\Omega\frac{\Omega^2-8\Delta^2}{\Omega-\sqrt{\Omega^2-8\Delta^2}}}. \quad (42)$$

The red area corresponds to the overdamping regime. Here, the intersection point of b_1 and b_2 is $(\frac{\gamma}{\Omega}, \frac{\Delta}{\Omega}) = (\frac{9}{\sqrt{6}}, \frac{1}{2\sqrt{2}})$, while the intersection point of b_1 and b_3 is $(\frac{\gamma}{\Omega}, \frac{\Delta}{\Omega}) = (\frac{9}{\sqrt{6}}, -\frac{1}{2\sqrt{2}})$.

The phase diagram is useful for clock frequency estimation. When the system is in the overdamping regime, the population will not oscillate and one will not be able to determine the clock frequency. Therefore, to extract the clock frequency via the population oscillation under spontaneous emission, one should ensure that the system is always in the damped oscillating regimes. The spontaneous emission rate should satisfy the following condition:

$$0 < \gamma < \sqrt{14\Omega^2 - 4\Delta^2 + 4\Omega\frac{\Omega^2-8\Delta^2}{\Omega+\sqrt{\Omega^2-8\Delta^2}}}, \quad (43)$$

i.e., γ should be on the left side of curve b_2 in Fig. 2.

Meanwhile, the corresponding analytic solution can be given as (derived from Sections 2.2 and 2.3)

$$w^Q(t) = C_1 e^{\lambda_1 t} + e^{\eta t}[C_2\cos(\omega t) + C_3\sin(\omega t)] + w_s^Q(t). \quad (44)$$

Here, $w_s^Q(t) = -\frac{4\Delta^2+\gamma^2}{4\Delta^2+\gamma^2+2\Omega^2}e^{\gamma t}$, $\lambda_1 = \frac{1}{3}\gamma + R_1 + R_2$, $\eta = \frac{1}{3}\gamma - \frac{1}{2}(R_1+R_2)$ and $\omega = \frac{\sqrt{3}}{2}(R_1 - R_2)$ with $R_1 = (-\frac{1}{2}q + \sqrt{D})^{1/3}$, $R_2 = (-\frac{1}{2}q - \sqrt{D})^{1/3}$, $p = \Delta^2 + \Omega^2 - \frac{1}{12}\gamma^2$, $q = \frac{1}{108}\gamma(36\Delta^2 - 18\Omega^2 + \gamma^2)$, and $D = \frac{1}{4}q^2 + \frac{1}{27}p^3$. The coefficients (C_1, C_2, C_3) are obtained by the solution of a linear equation (see Appendix B),

$$\begin{pmatrix} \lambda_1^2 & \eta^2-\omega^2 & 2\eta\omega \\ \lambda_1 & \eta & \omega \\ 1 & 1 & 0 \end{pmatrix}\begin{pmatrix} C_1 \\ C_2 \\ C_3 \end{pmatrix} = \begin{pmatrix} B_1 \\ B_2 \\ B_3 \end{pmatrix}, \quad (45)$$

where $B_1 = -\Delta\Omega u_0 + \frac{1}{2}\Omega\gamma v_0 - \Omega^2 w_0 - (w_0^Q + 1)\gamma^2$, $B_2 = \Omega v_0 - (w_0^Q + 1)\gamma$, and $B_3 = w_0 - w_0^Q$ with $w_0^Q = w_s^Q(0)$.

3.2 Clock frequency estimation in damped oscillating regime

In this section, we discuss the method in which to estimate the clock frequency of the TLS in the presence of spontaneous emission. The TLS initials from $|g\rangle$ at time $t = 0$ and the population will oscillate when the driving field is applied. Substituting the initial condition

$(u_0, v_0, w_0)^{\mathrm{T}} = (0, 0, -1)^{\mathrm{T}}$ into Eq. (12), we have

$$\begin{cases} \langle \hat{\sigma}^x \rangle = \cos(\omega_0 t)u(t) - \sin(\omega_0 t)v(t), \\ \langle \hat{\sigma}^y \rangle = \sin(\omega_0 t)u(t) + \cos(\omega_0 t)v(t), \\ \langle \hat{\sigma}^z \rangle = w(t), \end{cases} \quad (46)$$

where $\langle \hat{\sigma}^z \rangle$ represents the population difference between $|e\rangle$ and $|g\rangle$. When γ is moderate and satisfies Eq. (43), the system is in the damped oscillating regime and the evolved excited population $P_e(t)$ is expressed as

$$P_e(t) = \frac{1 + \langle \hat{\sigma}^z \rangle}{2} = \frac{1 + w(t)}{2} = \frac{1 + w^Q(t)\mathrm{e}^{-\gamma t}}{2}, \quad (47)$$

with $w^Q(t)$ being given according to Eq. (44). Here, the evolution of the excited population $P_e(t)$ is determined by both the detuning Δ and spontaneous emission rate γ.

If the system is at resonance, i.e., $\omega_D = \omega_0$, the spontaneous emission shrinks the amplitude (or the contrast) of the excited population [see Fig. 3 (a)]. When $\gamma = 0$, the excited population oscillates sinusoidally from 0 to 1 with Rabi frequency Ω. When $\gamma > 0$, the excited population oscillates with damped amplitudes. The excited population will cease to oscillate when the evolution time is sufficiently long. As γ increases, the maximum amplitude decreases rapidly.

The detuning affects both the amplitude (or the contrast) and period of $P_e(t)$. The evolution of the excited population with different detunings under $\gamma = 0.005$ is shown in Fig. 3(b). As the detuning Δ increases, the maximum amplitude drops and the oscillation period decreases.

From the responses of the excited population with different driving frequencies ω_D, one can extract the information of the clock frequency ω_0. We calculate the evolved excited population with different detunings Δ and determine the maximum amplitude $P_{e,\max}$. In Fig. 3(c), we show the spectrum of maximum excited population $P_{e,\max}$ versus detuning Δ with different spontaneous emission rates γ. The peaks with different γ are all centered at $\Delta = 0$, which indicates that no additional frequency shift is induced by the spontaneous emission and ω_0 can be determined by tuning the driving frequency ω_D with the largest $P_{e,\max}$.

However, the height of the peak decreases as the effects of spontaneous emission become stronger. The peak also becomes less sharp when γ increases. This implies that the process of spontaneous emission would have a negative influence on the estimated precision of ω_0. To characterize the estimated precision of ω_0 quantitatively, we use the full width at half maximum (FWHM) of the spectrum denoted by $\Delta\omega_{\mathrm{FWHM}}$. In the inset of Fig. 3(c), we show the dependence of the relative FWHM $\Delta\tilde{\omega}_{\mathrm{FWHM}}$ on

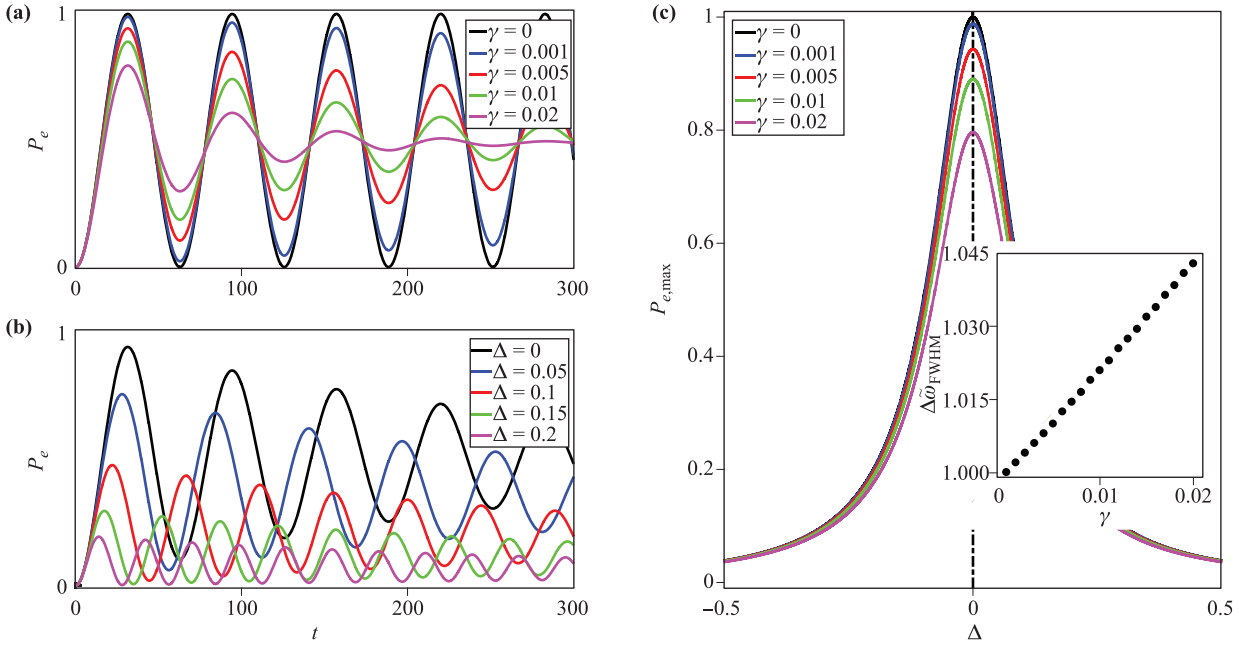

Fig. 3 **(a)** Evolution of excited population at resonance ($\Delta = 0$) under different spontaneous emission rates $\gamma = 0$ (*black*), 0.001 (*blue*), 0.005 (*red*), 0.01 (*green*), and 0.02 (*magenta*). **(b)** Evolution of excited population under spontaneous emission ($\gamma = 0.005$) with different detunings $\Delta = 0$ (*black*), 0.05 (*blue*), 0.1 (*red*), 0.15 (*green*), and 0.2 (*magenta*). **(c)** Spectrum of maximum excited population versus detuning Δ under different spontaneous emission rates $\gamma = 0$ (*black*), 0.001 (*blue*), 0.005 (*red*), 0.01 (*green*), and 0.02 (*magenta*). The inset shows the relationship of the relative full-width at half-maximum of the spectrum $\Delta\tilde{\omega}_{\mathrm{FWHM}}$ versus spontaneous emission rate γ. Here, we set $\omega_0 = 10$ and $\Omega = 0.1$.

the spontaneous emission γ. Here, the relative FWHM is defined as the FWHM with respect to that for $\gamma = 0$:

$$\Delta\tilde{\omega}_{\mathrm{FWHM}}(\gamma) = \frac{\Delta\omega_{\mathrm{FWHM}}(\gamma)}{\Delta\omega_{\mathrm{FWHM}}(\gamma = 0)}. \tag{48}$$

It can be observed that $\Delta\tilde{\omega}_{\mathrm{FWHM}}$ increases with γ, indicating that the estimated precision of the clock frequency becomes worse when the spontaneous emission gradually comes into play. Although the spontaneous emission reduces the measurement precision, the clock frequency is not shifted and can still be estimated when the spontaneous emission rate is moderate.

4 Summary

In summary, we have explored the dynamical evolution of a driven TLS under spontaneous emission and illustrated the methods in which to perform clock frequency estimation based on this model. We derive the Bloch equations for the Lindblad equations in the Dirac picture and give the complete and exact analytical solutions with closed-form expressions. In the absence of spontaneous emission, our results recover the perfect Rabi oscillation. In the presence of spontaneous emission, the system may be in the damped oscillating or overdamping regime depending on both the spontaneous emission rate and detuning. We analytically derive the boundaries of these regimes and show how a driven TLS under spontaneous emission can be used for clock frequency estimation. We find that the spontaneous emission does not cause additional frequency shifts but reduces the estimated precision. Our results enable potential applications in the quantum frequency estimation [27–30] and quantum control [31–35] of driven TLSs under spontaneous emission.

Acknowledgements This work was supported by the National Natural Science Foundation of China (Grant Nos. 11374375, 11574405, and 11465008). Jiahao Huang was partially supported by the National Postdoctoral Program for Innovative Talents of China (Grant No. BX201600198).

Appendix A Coefficients for analytical solutions of Lindblad equation under $\Delta = 0$

The coefficients appearing in the solutions to the Lindblad equation are determined by the initial conditions $\boldsymbol{R}^Q(t=0) = \boldsymbol{R}(t=0) = (u_0, v_0, w_0)^{\mathrm{T}}$ with $u_0, v_0, w_0 \in \mathbb{R}$. We denote $g(t) = w^Q(t) - f_0 \mathrm{e}^{\gamma t}$ and $f_0 = -\frac{\gamma^2}{\gamma^2+2\Omega^2}$. As

$$\begin{cases} u^Q(t) = u_0 \mathrm{e}^{\frac{1}{2}\gamma t}, \\ v^Q(t) = \dfrac{1}{\Omega}[g'(t) + \gamma(f_0+1)\mathrm{e}^{\gamma t}], \\ w^Q(t) = g(t) + f_0 \mathrm{e}^{\gamma t}, \end{cases} \tag{A1}$$

we have

$$\begin{pmatrix} g'(0) \\ g(0) \end{pmatrix} = \begin{pmatrix} \Omega v_0 - \gamma(f_0+1) \\ w_0 - f_0 \end{pmatrix}. \tag{A2}$$

Thus, the coefficients (C_1, C_2) satisfy
(i) for $D_0 > 0$,

$$\begin{pmatrix} \lambda_1 & \lambda_2 \\ 1 & 1 \end{pmatrix} \begin{pmatrix} C_1 \\ C_2 \end{pmatrix} = \begin{pmatrix} g'(0) \\ g(0) \end{pmatrix}; \tag{A3}$$

(ii) for $D_0 = 0$,

$$\begin{pmatrix} \eta & 1 \\ 1 & 0 \end{pmatrix} \begin{pmatrix} C_1 \\ C_2 \end{pmatrix} = \begin{pmatrix} g'(0) \\ g(0) \end{pmatrix}; \tag{A4}$$

(iii) for $D_0 < 0$,

$$\begin{pmatrix} \eta & \omega \\ 1 & 0 \end{pmatrix} \begin{pmatrix} C_1 \\ C_2 \end{pmatrix} = \begin{pmatrix} g'(0) \\ g(0) \end{pmatrix}. \tag{A5}$$

Solving the linear equations (A3), (A4), and (A5) gives the values for the coefficients (C_1, C_2). Here, we only give results for $D_0 < 0$, which is concerned in the main text:

$$\begin{cases} C_1 = w_0 - f_0, \\ C_2 = \dfrac{1}{\omega}[\Omega v_0 - \eta(w_0 - f_0) - \gamma(f_0+1)]. \end{cases} \tag{A6}$$

Appendix B Coefficients for analytical solutions of Lindblad equation under $\Delta \neq 0$

Similar to Appendix A, we denote $g(t) = w^Q(t) - f_0 e^{\gamma t}$, $f_0 = -\frac{4\Delta^2+\gamma^2}{4\Delta^2+\gamma^2+2\Omega^2}$, and $f_1 = -\frac{4\Delta^2\Omega^2}{4\Delta^2+\gamma^2+2\Omega^2}$. As

$$\begin{cases} u^Q(t) = -\dfrac{1}{\Delta\Omega}\left[g''(t) - \dfrac{1}{2}\gamma g'(t) + \Omega^2 g(t) + f_1 \mathrm{e}^{\gamma t}\right], \\ v^Q(t) = \dfrac{1}{\Omega}[g'(t) + \gamma(f_0+1)\mathrm{e}^{\gamma t}], \\ w^Q(t) = g(t) + f_0 \mathrm{e}^{\gamma t}, \end{cases} \tag{B1}$$

we have

$$\begin{pmatrix} g''(0) \\ g'(0) \\ g(0) \end{pmatrix} = \begin{pmatrix} -\Omega\left(\Delta u_0 - \dfrac{1}{2}\gamma v_0 + \Omega w_0\right) - \gamma^2(f_0+1) \\ \Omega v_0 - \gamma(f_0+1) \\ w_0 - f_0 \end{pmatrix}. \tag{B2}$$

Thus, the coefficients (C_1, C_2, C_3) satisfy
(i) for $D = 0$ and $p = 0$,

$$\begin{pmatrix} \eta^2 & 2\eta & 2 \\ \eta & 1 & 0 \\ 1 & 0 & 0 \end{pmatrix} \begin{pmatrix} C_1 \\ C_2 \\ C_3 \end{pmatrix} = \begin{pmatrix} g''(0) \\ g'(0) \\ g(0) \end{pmatrix}; \tag{B3}$$

(ii) for $D = 0$ and $p \neq 0$,

$$\begin{pmatrix} \lambda_1^2 & \lambda_2^2 & 2\lambda_2 \\ \lambda_1 & \lambda_2 & 1 \\ 1 & 1 & 0 \end{pmatrix} \begin{pmatrix} C_1 \\ C_2 \\ C_3 \end{pmatrix} = \begin{pmatrix} g''(0) \\ g'(0) \\ g(0) \end{pmatrix}; \tag{B4}$$

(iii) for $D < 0$,

$$\begin{pmatrix} \lambda_1^2 & \lambda_2^2 & \lambda_3^2 \\ \lambda_1 & \lambda_2 & \lambda_3 \\ 1 & 1 & 1 \end{pmatrix} \begin{pmatrix} C_1 \\ C_2 \\ C_3 \end{pmatrix} = \begin{pmatrix} g''(0) \\ g'(0) \\ g(0) \end{pmatrix}; \tag{B5}$$

(iv) for $D > 0$,

$$\begin{pmatrix} \lambda_1^2 & \eta^2 - \omega^2 & 2\eta\omega \\ \lambda_1 & \eta & \omega \\ 1 & 1 & 0 \end{pmatrix} \begin{pmatrix} C_1 \\ C_2 \\ C_3 \end{pmatrix} = \begin{pmatrix} g''(0) \\ g'(0) \\ g(0) \end{pmatrix}. \tag{B6}$$

Solving the linear equations (B3), (B4), (B5), and (B6) gives the values for the coefficients (C_1, C_2, C_3). Here, we only give the results for $D > 0$, which is concerned in the main text:

$$\begin{cases} C_1 = -\dfrac{\Omega\Delta}{(\lambda_1-\eta)^2+\omega^2} u_0 + \dfrac{\Omega(\frac{1}{2}\gamma - 2\eta)}{(\lambda_1-\eta)^2+\omega^2} v_0 \\ \qquad + \dfrac{\eta^2+\omega^2-\Omega^2}{(\lambda_1-\eta)^2+\omega^2} w_0 + \dfrac{\gamma(2\eta-\gamma)(f_0+1) - f_0(\eta^2+\omega^2)}{(\lambda_1-\eta)^2+\omega^2}, \\ C_2 = w_0 - f_0 - C_1, \\ C_3 = \dfrac{1}{\omega}\left[\Omega v_0 - \eta(w_0 - f_0) - \gamma(f_0+1) + (\eta - \lambda_1) C_1\right]. \end{cases} \tag{B7}$$

The results in Section 2.3 and Appendix B are for $\Delta \neq 0$. However, the calculations should also be applicable for $\Delta = 0$. To reveal this point, we assume $\Delta = 0$ in the following discussion. As $\Delta = 0$, we have $q = \frac{1}{108}\gamma(\gamma^2 - 18\Omega^2)$, $D = -\frac{1}{108}\Omega^4 D_0$ $(D_0 = \frac{1}{4}\gamma^2 - 4\Omega^2)$, and $\omega = \frac{\sqrt{3}}{2}\left[(-\frac{q}{2} + \sqrt{D})^{1/3} + (\frac{q}{2} + \sqrt{D})^{1/3}\right]$. Introducing $x = \frac{1}{2\Omega}\sqrt{-D_0}$ (where $0 < x \leq 1$), we have $D_0 = -4\Omega^2 x^2$, $D = \frac{1}{27}\Omega^6 x^2$, $\gamma = 4\Omega\sqrt{1-x^2}$, $q = -\frac{2}{27}\Omega^3(1+8x^2)\sqrt{1-x^2}$, and

$$\omega = \frac{1}{2}\Omega\,(S_1 + S_2)\,. \tag{B8}$$

Here, we introduce

$$\begin{cases} S_1 = \left[x + \dfrac{\sqrt{3}}{9}(1+8x^2)\sqrt{1-x^2}\right]^{1/3}, \\ S_2 = \left[x - \dfrac{\sqrt{3}}{9}(1+8x^2)\sqrt{1-x^2}\right]^{1/3}. \end{cases} \tag{B9}$$

Then, $S_1 + S_2 = \frac{2\omega}{\Omega}$ and $S_1 S_2 = \frac{1}{3}(4x^2 - 1)$. By $(S_1 + S_2)^3 = S_1^3 + S_2^3 + 3S_1S_2(S_1 + S_2)$, we have $(\frac{2\omega}{\Omega})^3 = 2x + (4x^2 - 1)\frac{2\omega}{\Omega}$, i.e., $(\omega - \Omega x)(4\omega^2 + 4\omega\Omega x + \Omega^2) = 0$. Therefore,

$$\omega = \Omega x = \frac{1}{2}\sqrt{-D_0}. \tag{B10}$$

Similarly, $\eta = \frac{1}{3}\gamma - \frac{1}{2}(R_1 + R_2) = \frac{1}{4}\gamma$. As $\Delta = 0$, $\frac{1}{2}\gamma - 2\eta = 0$, $\eta^2 + \omega^2 - \Omega^2 = 0$, and $\gamma(2\eta - \gamma)(f_0 + 1) - f_0(\eta^2 + \omega^2) = 0$, we have

$$\begin{cases} C_1 = 0, \\ C_2 = w_0 - f_0, \\ C_3 = \dfrac{1}{\omega}\left[\Omega v_0 - \eta(w_0 - f_0) - \gamma(f_0 + 1)\right] \end{cases} \tag{B11}$$

[from Eq. (B7)]. All these recover the results in Section 2.2 and Appendix A.

References

1. J. L. Hall, Nobel lecture: Defining and measuring optical frequencies, *Rev. Mod. Phys.* 78(4), 1279 (2006)
2. T. W. Hänsch, Nobel lecture: Passion for precision, *Rev. Mod. Phys.* 78(4), 1297 (2006)
3. H. Margolis, Timekeepers of the future, *Nat. Phys.* 10(2), 82 (2014)
4. M. Takamoto and H. Katori, Spectroscopy of the $^1S_0 - {}^3P_0$ clock transition of ^{87}Sr in an optical lattice, *Phys. Rev. Lett.* 91(22), 223001 (2003)
5. T. Steinmetz, T. Wilken, C. Araujo-Hauck, R. Holzwarth, T. W. Hänsch, L. Pasquini, A. Manescau, S. D'Odorico, M. T. Murphy, T. Kentischer, W. Schmidt, and T. Udem, Laser frequency combs for astronomical observations, *Science* 321(5894), 1335 (2008)
6. M. S. Grewal, A. P. Andrews, and C. G. Bartone, Global Navigation Satellite Systems, Inertial Navigation, and Integration, New York: John Wiley & Sons, 2013
7. J. Kitching, S. Knappe, and E. A. Donley, Atomic sensors – A review, *IEEE Sens. J.* 11(9), 1749 (2011)
8. D. Budker and M. Romalis, Optical magnetometry, *Nat. Phys.* 3(4), 227 (2007)
9. I. I. Rabi, Space quantization in a gyrating magnetic field, *Phys. Rev.* 51(8), 652 (1937)
10. N. Hinkley, J. A. Sherman, N. B. Phillips, M. Schioppo, N. D. Lemke, K. Beloy, M. Pizzocaro, C. W. Oates, and A. D. Ludlow, An atomic clock with 10^{-18} instability, *Science* 341(6151), 1215 (2013)
11. B. J. Bloom, T. L. Nicholson, J. R. Williams, S. L. Campbell, M. Bishof, X. Zhang, W. Zhang, S. L. Bromley, and J. Ye, An optical lattice clock with accuracy and stability at the 10^{-18} level, *Nature* 506(7486), 71 (2014)

12. T. L. Nicholson, S. L. Campbell, R. B. Hutson, G. E. Marti, B. J. Bloom, R. L. McNally, W. Zhang, M. D. Barrett, M. S. Safronova, G. F. Strouse, W. L. Tew, and J. Ye, Systematic evaluation of an atomic clock at 2×10^{-18} total uncertainty, *Nat. Commun.* 6, 6896 (2015)
13. S. G. Porsev and A. Derevianko, Multipolar theory of blackbody radiation shift of atomic energy levels and its implications for optical lattice clocks, *Phys. Rev. A* 74(2), 020502(R) (2006)
14. A. V. Taichenachev, V. I. Yudin, V. D. Ovsiannikov, and V. G. Pal'chikov, Optical lattice polarization effects on hyperpolarizability of atomic clock transitions, *Phys. Rev. Lett.* 97(17), 173601 (2006)
15. K. Gibble, Decoherence and collisional frequency shifts of trapped bosons and fermions, *Phys. Rev. Lett.* 103(11), 113202 (2009)
16. T. Rosenband, D. B. Hume, P. O. Schmidt, C. W. Chou, A. Brusch, L. Lorini, W. H. Oskay, R. E. Drullinger, T. M. Fortier, J. E. Stalnaker, S. A. Diddams, W. C. Swann, N. R. Newbury, W. M. Itano, D. J. Wineland, and J. C. Bergquist, Frequency ratio of Al^+ and Hg^+ single-ion optical clocks; metrology at the 17th decimal place, *Science* 319(5871), 1808 (2008)
17. C. W. Chou, D. B. Hume, J. C. J. Koelemeij, D. J. Wineland, and T. Rosenband, Frequency comparison of two high-accuracy Al^+ optical clocks, *Phys. Rev. Lett.* 104(7), 070802 (2010)
18. N. Huntemann, C. Sanner, B. Lipphardt, C. Tamm, and E. Peik, Single-ion atomic clock with 3×10^{-18} systematic uncertainty, *Phys. Rev. Lett.* 116(6), 063001 (2016)
19. S. Weinberg, Lindblad decoherence in atomic clocks, *Phys. Rev. A* 94(4), 042117 (2016)
20. E. Barnes and S. Das Sarma, Analytically solvable driven time-dependent two-level quantum systems, *Phys. Rev. Lett.* 109(6), 060401 (2012)
21. L. D. Landau, On the theory of transfer of energy at collisions II, *Phys. Z. Sowjetunion* 2, 46 (1932)
22. C. Zener, Non-adiabatic crossing of energy levels, *Proc. R. Soc. Lond. A* 137(833), 696 (1932)
23. L. Allen and J. H. Eberly, Optical Resonance and Two-Level Atoms, New York: Dover Publications, 1987
24. R. W. Boyd, Nonlinear Optics, Boston: Academic Press, 1992
25. P. Meystre, Atom Optics, New York: Springer-Verlag, 2001
26. S. Haroche and J. M. Raimond, Exploring the Quantum: Atoms, Cavities, and Photons, New York: Oxford University Press, 2006
27. P. A. Ivanov and D. Porras, Adiabatic quantum metrology with strongly correlated quantum optical systems, *Phys. Rev. A* 88(2), 023803 (2013)
28. N. Malossi, M. G. Bason, M. Viteau, E. Arimondo, D. Ciampini, R. Mannella, and O. Morsch, Quantum driving of a two level system: Quantum speed limit and superadiabatic protocols – an experimental investigation, *J. Phys. Conf. Ser.* 442(1), 012062 (2013)
29. Z. Tian, J. Wang, H. Fan, and J. Jing, Relativistic quantum metrology in open system dynamics, *Sci. Rep.* 5(1), 7946 (2015)
30. P. A. Ivanov, K. Singer, N. V. Vitanov, and D. Porras, Quantum sensors assisted by spontaneous symmetry breaking for detecting very small forces, *Phys. Rev. Appl.* 4(5), 054007 (2015)
31. A. Greilich, S. E. Economou, S. Spatzek, D. R. Yakovlev, D. Reuter, A. D. Wieck, T. L. Reinecke, and M. Bayer, Ultrafast optical rotations of electron spins in quantum dots, *Nat. Phys.* 5(4), 262 (2009)
32. E. Poem, O. Kenneth, Y. Kodriano, Y. Benny, S. Khatsevich, J. E. Avron, and D. Gershoni, Optically induced rotation of an exciton spin in a semiconductor quantum dot, *Phys. Rev. Lett.* 107(8), 087401 (2011)
33. M. G. Bason, M. Viteau, N. Malossi, P. Huillery, E. Arimondo, D. Ciampini, R. Fazio, V. Giovannetti, R. Mannella, and O. Morsch, High-fidelity quantum driving, *Nat. Phys.* 8(2), 147 (2011)
34. S. Sauer, C. Gneiting, and A. Buchleitner, Optimal coherent control to counteract dissipation, *Phys. Rev. Lett.* 111(3), 030405 (2013)
35. D. Daems, A. Ruschhaupt, D. Sugny, and S. Guérin, Robust quantum control by a single-shot shaped pulse, *Phys. Rev. Lett.* 111(5), 050404 (2013)
36. Y. Wu and X. Yang, Strong-coupling theory of periodically driven two-level systems, *Phys. Rev. Lett.* 98(1), 013601 (2007)
37. X. Yang and Y. Wu, Weak-coupling theory for semiclassical periodically driven two-level systems: Beyoud rotating-wave approximation, *Commum. Theor. Phys.* 48(2), 339 (2007)
38. Q. Xie and W. Hai, Analytical results for a monochromatically driven two-level system, *Phys. Rev. A* 82(3), 032117 (2010)
39. W. Hai, K. Hai, and Q. Chen, Transparent control of an exactly solvable two-level system via combined modulations, *Phys. Rev. A* 87(2), 023403 (2013)
40. E. Barnes, Analytically solvable two-level quantum systems and Landau-Zener interferometry, *Phys. Rev. A* 88(1), 013818 (2013)
41. A. Messina and H. Nakazato, Analytically solvable Hamiltonians for quantum two-level systems and their dynamics, *J. Phys. A Math. Theor.* 47(44), 445302 (2014)
42. H. P. Breuer and F. Petruccione, The Theory of Open Quantum Systems, New York: Oxford University Press, 2002
43. M. A. Nielsen and I. L. Chuang, Quantum Computation and Quantum Information, Cambridge: Cambridge University Press, 2000
44. M. Grifoni and P. Hänggi, Driven quantum tunneling, *Phys. Rep.* 304(5–6), 229 (1998)

45. M. Thorwart, L. Hartmann, I. Goychuk, and P. Hänggi, Controlling decoherence of a two-level atom in a lossy cavity, *J. Mod. Opt.* 47(14–15), 2905 (2000)

46. D. Mogilevtsev, A. P. Nisovtsev, S. Kilin, S. B. Cavalcanti, H. S. Brandi, and L. E. Oliveira, Driving-dependent damping of Rabi oscillations in two-level semiconductor systems, *Phys. Rev. Lett.* 100(1), 017401 (2008)

47. A. Sergi and K. G. Zloshchastiev, Non-Hermitian quantum dynamics of a two-level system and models of dissipative environments, *Int. J. Mod. Phys. B* 27(27), 1350163 (2013)

48. K. N. Zlatanov, G. S. Vasilev, P. A. Ivanov, and N. V. Vitanov, Exact solution of the Bloch equations for the nonresonant exponential model in the presence of dephasing, *Phys. Rev. A* 92(4), 043404 (2015)

49. M. S. P. Eastham, The Spectral Theory of Periodic Differential Equations, Edinburgh and London: Scottish Academic Press, 1973